Iranian Journal of Medical Physics
Vol. 11, No. 2 & 3, Spring & Summer 2014, 284-293
Received: November 3, 2013; Accepted: January 16, 2014

Original Article

Automatic Sperm Analysis in Microscopic Images of Human Semen: Segmentation Using Minimization of Information Distance

Seyed Vahab Shojaedini[1*], Masoud Heydari[1]

Abstract

Introduction
The morphologic features of human sperms are key indicators for monitoring fertility problems in men. Therefore, automated analyzing methods via microscopic videos have become the most favorite policy in infertility treatment during the last decades.
Materials and Methods
In the proposed method, firstly a hypothesis testing framework was defined to distinguish sperms from background. Then, some regions were selected as candidates by minimization of the information distance between the original and processed images. Finally, the correct sperms were extracted from candidates using a watershed-based algorithm.
Results
The proposed, Watershed Segmentation Algorithm (WSA), Multi Structure Element Segmentation (MSES) and Dynamic Threshold Segmentation (DTS) algorithms achieve true positive rates of 96%, 84%, 81%, and 70%, respectively, versus typically 3% of false positive rate in semen specimens with high density of sperms. The true positive rates of 87%, 69%, 66%, and 52%, respectively, at the same false positive rate were obtained for the semen specimens with high density of sperms.
Conclusion
Results show that false positive rates of the proposed algorithm were at least 8% (in the first scenario) and 32% (in the second scenario) better than other methods considering the minimum acceptable true positive rate of 90%. Furthermore, it has been shown that the proposed algorithm extracted sperms at least 12% (in the first scenario) and 18% (in the second scenario) better than other methods in presence of a typically low false positive rate equal to 3%.
Keywords: Entropy, Infertility, Microscopy, Semen, Spermatozoa.

1- *Electrical and Computer Engineering Department, Iranian Research Organization for Science and Technology, Tehran, Iran.*
*Corresponding author: Tel: +982156276344; E-mail: shojadini@irost.ir

1. Introduction

It is known that semen of men with impaired fertility has fewer sperms than the semen of men with normal fertility [1,2]. Moreover, it has been shown that abnormal morphology of sperms can be related with fertility hazards in men [3,4]. Therefore, analyzing the male semen in order to determine sperm population and morphology has become the most favorite policy of researchers in monitoring infertility [5,6]. In the recent years, microscopic imaging has been widely used for studying semen [7,8]. The most challenging step of this procedure is to separate sperms from other particles in semen microscopic images which is called sperm detection. During several years, manual sperm detection by an expert person has been the main technique to do such a separation. However, visual analyzing method is considerably effort-demanding and time-consuming. Furthermore, the inherent lack of objectivity in the evaluation of human sperm morphology in this method, leads to the high degree of variation between different laboratories and technicians [9].

Based on the aforementioned limitations, the automated sperm detection and analysis methods have been developed rapidly during last two decades [10]. The low contrast of the sperm under various microscopy conditions is a major challenge in automated methods. Despite the considerable amount of work that has been done in this field, automated detection of sperm has been remained as an open problem. Some methods try to detect sperms using information obtained from the sperm head. Unfortunately, this approach is not capable of extracting the sperm tail completely [11]. Since edge information cannot be extracted from microscopic images which are intrinsically low contrast, active contour-based sperm detection algorithms have been developed. However, these methods require several iterations which make them unsuitable for real-time applications. In some prior arts, threshold-based segmentation algorithms have been applied. These methods are very sensitive to values of the thresholds which are used for segmentation that leads to considerable missing of sperms or false detections [12].

In some other researches, detecting human sperms is performed using the region growing algorithms. Unfortunately, these methods often lead to merging the neighboring sperms [13]. As for more sophisticated methods, various types of matching can be named. In these methods, constant or flexible masks are used to separate sperms from other parts of semen. These approaches suffer from some limitations such as high sensitivity to shape, size, and rotation of sperms [14].

In some researches, the wavelet transform has been utilized to distinguish sperms from other parts of semen. Despite the capability of this method in extracting sperm morphology, its performance is degraded considerably in semen specimens with high density of sperms [15]. Some methods utilize watershed segmentation for separating sperms from other specimens of semen. Although these methods may estimate the existence of sperm, they may not determine an exact boundary between it and background. Therefore, the above methods may not extract sperm morphology as well [16].

In this paper, a sperm detection technique based on minimization of the information distance between the original and processed image, followed by watershed segmentation method is presented. In the proposed method, firstly, the co-occurrence matrix was calculated which contains information on the distribution of gray level transition frequency. Using elements of this matrix, the entropy of transitions across boundaries of image contents were calculated which indicates some regions of image as primary “candidates” for sperms. Finally, an algorithm which is based on watershed segmentation was applied to determine complete sperms from the above candidates. Unlike the existing methods, the proposed algorithm extracts more accurate morphology for sperms in high density semen specimens. This advantage arises from the ability of the the proposed algorithm in removing background of microscopic images.

The paper is organized as follows. In section II, the proposed algorithm is introduced including entropy-based candidate selection followed by watershed-based segmentation. In section III, the performance of the proposed method is evaluated in two different scenarios based on real microscopic images of semen specimens. In section IV, the obtained results from experiments are compared with results of some existing methods using their effective parameters. Conclusion is presented in the last section of the paper.

2. Materials and Methods

Suppose I as a microscopic image captured from a semen specimen which contains sperms, plasma, and debris which two latter parameters are called background in this article. For each pixel of I it can be written:

$$I_{lj} = I(l, j) \quad 1 \le l \le L \quad , \quad 1 \le j \le J \tag{1}$$

In which, I_{lj} is brightness of a pixel which is located in row and column equal with l and j, respectively. Moreover, L and J are image sizes. Dependence of the pixel I_{lj} to background, noise, or sperm is modeled by hypothesis testing equation (2):

$$\begin{cases} H_0 : & I_{lj} = \left| c_{lj} + n_{lj} \right| \\ H_1 : & I_{lj} = \left| r_{lj} + c_{lj} + n_{lj} \right| \end{cases} \tag{2}$$

In the above equation, r_{lj}, c_{lj} and n_{lj} show the sperm, background, and noise components in I_{lj}, respectively.

2.1. Mathematical Description of the Method

Assume that I has N gray levels denoted by $\beta = \{0,1,2,...,N-1\}$ which constructs 1-D histogram of I. However, this 1-D histogram neglects the correlation among gray levels of sperms and background which is vital in segmentation of I. In order to resolve this problem, the co-occurrence matrix is introduced which is a square matrix as $W = [w_{km}]_{N*N}$ in which w_{km} is the numbers of transitions between all pairs of gray levels in β. The above parameter is defined as [17,18]:

$$w_{km} = \sum_{l=1}^{L} \sum_{j=1}^{J} \tau_{lj} \tag{3}$$

In which

$$\tau_{lj} = \begin{cases} 1 & if\ I_{lj} = k \ \ and \ \ I_{l+1,j} = m \\ 1 & if\ I_{lj} = k \ \ and \ \ I_{l,j+1} = m \\ 0 & otherwise \end{cases} \tag{4}$$

The transition probability from gray level k to gray level m is obtained as:

$$g_{km} = \frac{w_{km}}{\sum_{k'=0}^{N-1} \sum_{m'=0}^{N-1} w_{k'm'}} \tag{5}$$

Let T be a threshold used to separate sperms from other particles in microscopic image I. Therefore, it partitions co-occurrence matrix into four quadrants as A_1, A_2, A_3, and A_4. These four quadrants can be clustered into two classes. Let pixels with gray levels above the threshold be assigned to the sperms and those equal to or below the threshold are assigned to the background. Therefore, A_1 and A_3 show local transitions within background and sperms, which are called local quadrants. The quadrants A_2 and A_4 represent joint transitions across boundaries between background and sperms which are called joint quadrants. The probability of each quadrant is:

$$G_{A_1}^T = \sum_{k=0}^{T} \sum_{m=0}^{T} g_{km} \qquad G_{A_2}^T = \sum_{k=0}^{T} \sum_{m=T+1}^{N-1} g_{km}$$
$$G_{A_3}^T = \sum_{k=T+1}^{N-1} \sum_{m=0}^{T} g_{km} \qquad G_{A_4}^T = \sum_{k=T+1}^{N-1} \sum_{m=T+1}^{N-1} g_{km} \tag{6}$$

If the threshold T applied to the original image I it leads to processed image I'. Now, the transition probabilities of I are shown as $G = [g_{km}]_{N*N}$, and for the I' are shown as $F^T = [f_{km}^T]_{N*N}$, which f_{km}^T has the similar definition as g_{km}. The second-order entropy of

the above gray-level transition probabilities is defined as [19]:

$$E(G,F^T)=\sum_{k=0}^{N-1}\sum_{m=0}^{N-1}g_{km}\log\frac{g_{km}}{f_{km}^T} \quad (7)$$

The above entropy is used to measure the information distance between the original image I and the processed (e.g., thresholded) image I'. Therefore, the smaller this entropy is, the closer the two images are in terms of their probability distributions. Based on this fact, it can be concluded that minimization of $E(G,F^T)$ over T generates I' in such a way that best matches I. Let all gray levels above T are called $\beta_1=\{T+1,T+2,...,N-1\}$ and all gray levels equal to or below T are called $\beta_0=\{0,1,...,T\}$. Therefore, β_1 and β_0 are partitioned sets of β which had been introduced before. Assuming that the gray levels in β_1 and β_0 are uniformly distributed in their respective regions, the resulting f_{km}^T for each quadrant can be found by [20,21]:

$$f_{km|A_1}^T=\frac{G_{A_1}^T}{(T+1)(T+1)},\quad \forall k,m\in\beta_0$$

$$f_{km|A_2}^T=\frac{G_{A_2}^T}{(T+1)(N-T-1)},\forall k\in\beta_0,m\in\beta_1$$

$$f_{km|A_3}^T=\frac{G_{A_3}^T}{(N-T-1)(N-T-1)},\forall k\in\beta_1,m\in\beta_1$$

$$f_{km|A_4}^T=\frac{G_{A_4}^T}{(N-T-1)(T+1)},\forall k\in\beta_1,m\in\beta_0 \quad (8)$$

Where $G_{A_1}^T$, $G_{A_2}^T$, $G_{A_3}^T$, and $G_{A_4}^T$ were defined by (6). For a constant T, $f_{km|A_1}^T$, $f_{km|A_2}^T$, $f_{km|A_3}^T$, and $f_{km|A_4}^T$ are constants in each individual quadrant and they only depend upon which quadrants they belong to. To optimize equation (7) which leads to obtaining the best value of T, firstly, it is expanded as:

$$E(G,F^T)=E'([g_{km}])-\sum_{k=0}^{N-1}\sum_{m=0}^{N-1}g_{km}\log f_{km}^T=E'(G)-E''(T) \quad (9)$$

Where $E'(G)$ is the entropy of the probability matrix G and is independent of T. Moreover, $E''(T)$ is threshold-dependent part of entropy. As mentioned before, the best T is the one that yields the smallest value of $E(G,F^T)$. However, minimization of $E(G,F^T)$ in equation (9) is equivalent to maximizing the second term of the right-hand-side of this equation, which can be further reduced to:

$$E''(T)=G_{A_1}^T.\log(f_{km|A_1}^T)+G_{A_2}^T.\log(f_{km|A_2}^T)+G_{A_3}^T.\log(f_{km|A_3}^T)+G_{A_4}^T.\log(f_{km|A_4}^T) \quad (10)$$

Therefore, the threshold value T that maximizes (10) is mentioned as:

$$T=\arg\left\{\max_{T\in\beta}E''(T)\right\} \quad (11)$$

Let the result of thresholding by T be a processed image I' which is defined as:

$$\begin{cases}I'_{lj}=I_{lj} & I_{lj}>T\\ 0 & otherwise\end{cases} \quad (12)$$

Now suppose that $\chi_{I'_{\min}}$ denotes the union of the set of Q' local minimums of I' each of them can be considered a single object like as $O'_{q'}$:

$$\chi_{I'_{\min}}=\{O'_1,...,O'_{q'},...,O'_{Q'}\} \quad (13)$$

In which:

$$O'_{q'}=\{1\le l\le L,1\le j\le J\mid I'_{lj}=\min(Y_{lj})\} \quad (14)$$

In which Y_{lj} shows a window whose center is (l,j). Now, we consider the gray level $\alpha=I'_{lj}$. A neighbor of each member of $\chi_{I'_{\min}}$ can be either a new local minimum (e.g., add a member to $\chi_{I'_{\min}}$) or an extension of an existing object of $\chi_{I'_{\min}}$ (e.g. $O'_{q'}$). In the latter case, for each (l,j) which is four or eight connected to some members of $\chi_{I'_{\min}}$, like $O'_{q'}$ and $O'_{q''}$, geodesic influence zone of $\chi_{I'_{\min}}$ is computed as [21]:

$$Z(\chi_{I'_{\min}}) = \bigcup_{q'}^{Q'} Z'(O_{q'}', \chi_{I'_{\min}}) \quad (15)$$

In which:

$$Z'(O'_{q'}, \chi_{I'_{\min}}) = \{l, j \mid d(I'_{lj}, O'_{q'}) < \xi, \; d(I'_{lj}, O'_{q'}) < d(I'_{lj}, O'_{q''})\} \quad (16)$$

In above equation, $d(.)$ shows the distance and ξ shows gray level threshold for assigning pixel I'_{lj} to object $O'_{q'}$ or $O'_{q''}$. Now, the primary objects of $\chi_{I'_{\min}}$ may be updated. For this purpose, let γ_α denotes the union of all local minimums at level α which is not assigned by equations (14-16). Therefore, we have:

$$\chi_{I'_{lj}} = \chi_{I'_{\min}} \cup Z(\chi_{I'_{\min}}) \cup \gamma_\alpha \quad (17)$$

In the same manner, a recursion is defined with the gray level $\alpha = I'_{lj}$ increasing from $I'_{\min}$ to $I'_{\max}$ which are minimum and maximum levels in an image. In this recursion, the regions from $\chi_{I'_{\min}}$ to $\chi_{I'_{\max}}$ associated with the minimums of I' and successively expanded according to equations (18)-(20) which are general form of (15)-(17) [22,23].

$$\chi_{(\alpha+1)} = \chi_\alpha \cup Z(\chi_\alpha) \cup \gamma_{(\alpha+1)} \quad (18)$$

In which $Z(\chi_\alpha)$ is defined as:

$$Z(\chi_\alpha) = \bigcup_{q'}^{Q'} Z'(O_{q'}, \chi_\alpha) \quad (19)$$

And $Z'(O_{q'}, \chi_\alpha)$ is :

$$Z'(O'_{q'}, \chi_\alpha) = \{l, j \mid d(I'_{lj}, O'_{q'}) < \xi, \; d(I'_{lj}, O'_{q'}) < d(I'_{lj}, O'_{q''})\} \quad (20)$$

According to the above recursion, at level $\alpha + 1$, all non-assigned pixels are potential candidates to get assigned to objects who are members of χ_α. Therefore, it allows that pixels at gray level α which are not yet part of a sperm are merged with some sperms at the higher level $\alpha + 1$. Therefore, finally $\chi_{I'_{\max}}$ contains a set of clusters as:

$$\chi_{I'} = \chi_{I'_{\max}} = \{O_1, ..., O_q, ..., O_Q\} \quad (21)$$

Where O is the set of Q final expanded and merged sperms, (e.g., O_q) which are extracted from I'. By combining equations (2) and (21), dependence of each pixel to background and noise (H_0) or sperm (H_1) is determined as:

$$\begin{cases} H_0: \quad I_{lj} \notin O_q \;\; \Rightarrow I_{lj} = |c_{lj} + n_{lj}| \\ H_1: \quad I_{lj} \in O_q \;\; \Rightarrow I_{lj} = |r_{lj} + c_{lj} + n_{lj}| \end{cases} \quad (22)$$

2.2. Data Collection

The proposed algorithm was applied on microscopic videos which had been captured from human semen. The data collection setup contained a invert microscope(Nikon-Jappan) using a 100x zoom lens (Canon- Jappan) and an Orca ER digital CCD camera (Hamamatsu-Jappan) which had been mounted on the microscope to record videos. A calibrated microscope slide was used in all of the experiments. This microscope slide was scaled per 10 micrometer which enabled us to estimate size and movement parameters of sperms. After calibration, the semen sample was put on a non-scaled microscope slide and digital video was captured. The image of this non-scaled microscope slide existed in all captured frames as background. Therefore, the image of empty non-scaled microscope slide was subtracted from all captured frames for background elimination.

Using this procedure, 360 frames of semen were investigated which belonged to 11 infertile men. From this value, 180 pictures were associated to samples containing low density of sperms (i.e., bellow 2×10^6 sperms per milliliter) and the same number belonged to samples containing low density of sperms (i.e., more than 2×10^6 sperms per milliliter). Based on these populations, each of frames belonged to first scenario contained 41-73 sperms while each frames of the second scenario contained 136-221 sperms, both with average contrast equal to 17 percent. All captured frames had same sizes (i.e., 1344×1024 pixels) and each sperm included minimally 40 and maximally 190 pixels in an image.

3. Results

The proposed algorithm was applied on real data using Matlab (2009). Furthermore,

Watershed Segmentation Algorithm (WSA) [16], Multi Structure Element Segmentation (MSES) [24], and Dynamic Threshold Segmentation (DTS) [12] were also implemented to compare with the proposed algorithm. Tests were carried out on different scenarios which in one of them the semen specimens contained low densities of sperms and in another one specimens contained high densities of sperms. The captured videos were first processed using manual detection to obtain a ground-truth detection to compare the automatic methods with. Then, sperms were detected by applying the proposed and three other algorithms and finally performance of each algorithm was determined by comparing its results with manual detection results.

3.1. First scenario

In the first scenario, the captured images were obtained from semen specimens with densities bellow 2×10^6 sperms per milliliter. Two images of this scenario are shown in Figure 1. Figures 2 and 3 show obtained results utilizing the proposed and WSA methods on images of Figure 1. For instance, Figure 2-a shows that the proposed method has extracted 41 sperms from 43 original sperms which are shown in Figure 1-a with no false detection. Moreover, Figure 2-b shows that the proposed method has extracted 40 sperms of total 44 sperms which are shown in Figure 1-b again without any false detection. However, Figure 3 shows that WSA has weaker results than the proposed method. It is obvious in Figure 3-a that WSA has extracted 38 sperms from Figure 1-a. In the same manner, the results which are shown in Figure 3-b indicates that WSA has extracted 36 sperms correctly from Figure 1-b. These figures have not shown any false detection similar to 2-a and 2-b.

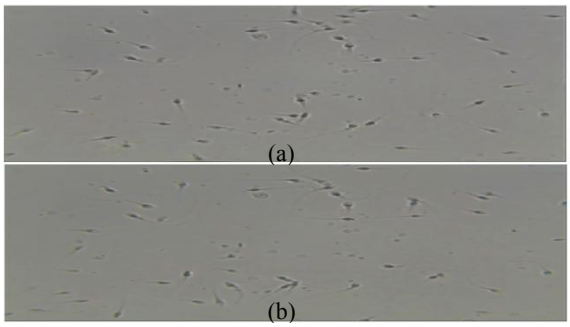

Figure 1. Two captured microscopic images for a semen specimen containing low density of sperms (first scenario).

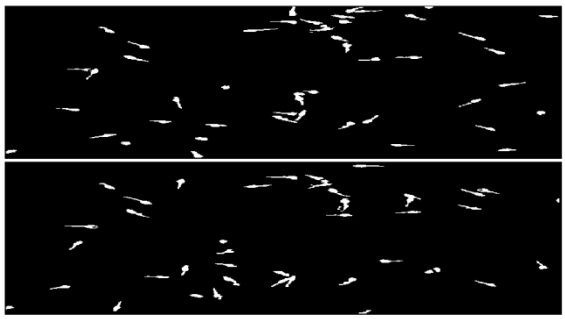
Figure 2. Extracted sperms by our method.


Figure 3. Extracted sperms by WSA method.

3.2. Second scenario

In this scenario, images were obtained from high density ($>2\times10^6$ sperms per milliliter) semen specimens. Such a high density caused some detection problems which the most important of them is merging sperms with near distances. Two examples for such images are shown in Figure 4. Figures 5 and 6 show results which were obtained from images of Figure 4 utilizing the proposed and WSA methods, respectively. For example, in Figure 5-a, it is shown that the proposed method has extracted 62 sperms from 69 original sperms in Figure 4-a also 2 false sperms have been detected. In the same way, Figure 5-b shows that the proposed method extracted 68 sperms

from a total 80 sperms in Figure 4-b plus 2 false sperms. Similar to the first scenario, WSA still has weaker results than the proposed method. This fact is shown in Figure 6. In Figure 6-a, it is obvious that WSA has extracted 51 sperms correctly from Figure 4-a and has 2 false detections. Figure 6-b shows above values equal with 56 correct and 2 false sperms after processing of Figure 4-b.

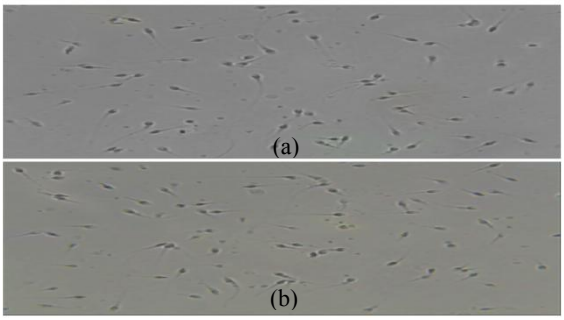

Figure 4. Two captured microscopic images for a semen specimen containing high density of sperms (second scenario).

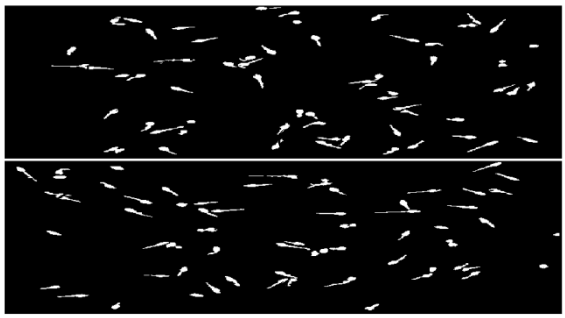

Figure 5. Extracted sperms by our method.

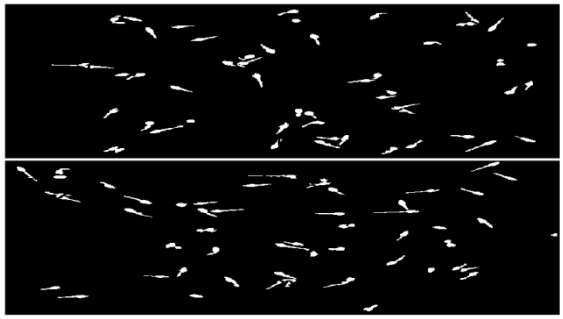

Figure 6. Extracted sperms by WSA method.

4. Discussion

In the current stydy, real data which were obtained from semen microscopy were analyzed. The proposed algorithm and three existing methods (WSA, MSES, and DTS) were applied and the results were compared with manual detection using two standard parameters. The first parameter is True Positive Rate (TPR) and is defined as the ratio of correctly identified sperms (i.e., true positives) to sum of correctly identified and incorrectly rejected sperms (i.e., false negatives) as:

$$TPR = \frac{TP}{TP + FN} \tag{23}$$

In which TP and FN represent true positives and false negatives, respectively. The second evaluation parameter is False Positive Rate (FPR) which is the ratio of incorrectly identified sperms (i.e., false positives) to sum of incorrectly identified and correctly rejected sperms (i.e., true negatives) as:

$$FPR = \frac{FP}{FP + TN} \tag{24}$$

In which FP and TN represent false positives and true negatives, respectively. Using the mentioned parameters, ROC curves were obtained for all examined methods. Figures 7 and 8 show changes of TPR versus FPR for first and second scenarios, respectively. These figures show clearly the superiority of the proposed method compared with other methods in both of scenarios.

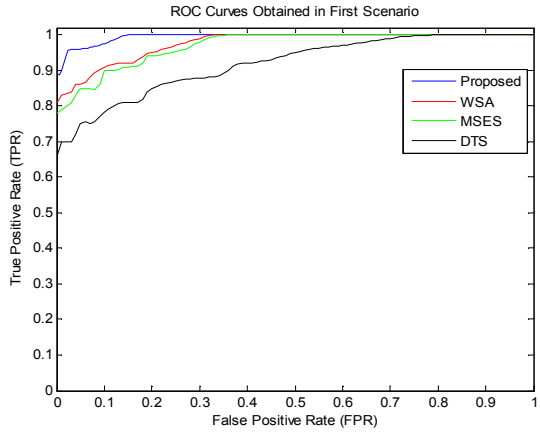

Figure 7. ROC curves obtained in first scenario for examined algorithms.

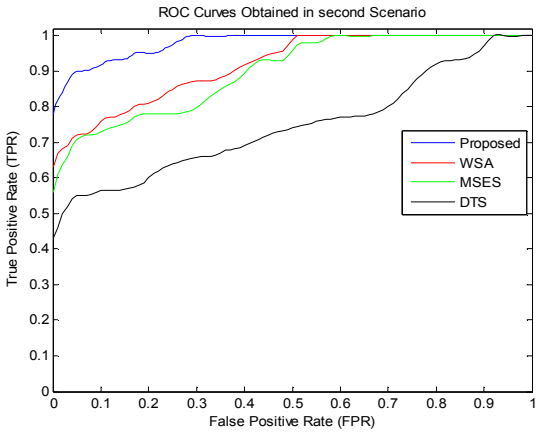

Figure 8. ROC curves obtained in second scenario for examined algorithms.

Firstly, the performances of algorithms were analyzed for an ideal case in which $FPR = 0\%$. As shown in Figure 7, in the first scenario, the values for false detections were 89%, 81%, 78%, and 66% of TPR for the proposed, WSA, MSES, and DTS algorithms, respectively. Similarly, Figure 8 shows TPR values equal to 80%, 63%, 56%, and 43% at the same FPR for the second scenario.

Another marginal situation belongs to the case of complete TPR. In this case, FPR values were equal to 15%, 33%, 38%, and 80% for the proposed, WSA, MSES, and DTS algorithms, respectively for the first scenario. Figure 8 shows that FPR values were equal to 29%, 52%, 59%, and 90% to achieve such a complete detection in second scenario.

To present a more practical interpretation, $FPR = 3\%$ was considered as a typical acceptable false detection value and the performances of algorithms were analyzed. As shown in Figure 7, the proposed, WSA, MSES, and DTS algorithms achieved TPR equal to 96%, 84%, 81%, and 70% versus this FPR in the first scenario. Similarly, Figure 8 shows TPR equal to 87%, 69%, 66%, and 52% at the same FPR for the second scenario. Based on these results, it can be concluded that having a typically low FPR (e.g., %3), the TPR of the proposed method is considerably (12% and 18% in first and second scenarios, respectively) higher than the best of three other methods (i.e., WSA). In another type of interpretation, the minimum acceptable value for TPR was considered equal to 90% to evaluate the performances of algorithms versus FPR. Under this condition, FPR values were 1%, 9%, 10%, and 36% for the proposed, WSA,MSES, and DTS algorithms in the first scenario (Figure 7). Similarly, FPR were equal to 6%, 38%, 41%, and 78% to achieve the threshold of $TPR = 90\%$ in second scenario (Figure 8). Therefore, it may be concluded that in the minimum acceptable TPR, the FPR of the proposed method were considerably (8% and 32% in first and second scenarios, respectively) better than other methods. Finally, it should be noted that due to more density of sperms in the second scenario, they have close proximity which led to degradation of results compared with the former scenario. ROC curves show that in the second scenario, TPR values were decreased at least 9% compared with the first scenario. In the same manner, FPR increased at least 5% in the second scenario compared with the first scenario. In spite of these degradations, the superiority of the proposed method versus other algorithms was more pronounced in the second scenario. The superior performance of the proposed algorithm versus the best of other algorithms (i.e., WSA) in TPR in the second scenario was 6% larger than its improvement in the first scenario. In the same manner, the superior performance of the proposed algorithm versus WSA in FPR in the second scenario was 24% better than its improvement versus WSA in the first scenario.

5. Conclusion

In this article, a new method was introduced for sperm detection in microscopic images of human semen. The proposed method is capable to distinguish sperms from other semen specimens using combination of entropy of transitions across boundaries and watershed-based segmentation. In order to evaluate the performance of the proposed algorithm, two scenarios were carried out based on real microscopic images of low and high densities of sperms. In both scenarios the performance of the proposed algorithm was

compared with three existing methods (i.e., WSA, MSES, and DTS) using their TPR and FPR. By exploiting the obtained ROC curves, the better performance of the proposed algorithm was proved. Results showed that the proposed algorithm extracted sperms at least 12% (in first scenario) and 18% (in second scenario) better than other methods in presence of a typically low FPR equal to 3%. Furthermore, it was shown that FPR values of the proposed algorithm were at least 8% (in first scenario) and 32% (in second scenario) better than other examined methods considering the minimum acceptable TPR of 90%. These results showed that better sperm detection achieved by the proposed algorithm did not increase FPR. Although the proposed algorithm showed a better performance compared with other examined algorithms, this superiority was more considerable in the second scenario. The aforementioned superiority in TPR in the second scenario was 6% however this superiority in FPR was 24%. Consequently, it can be concluded that the proposed method may be used as a suitable alternative for detecting sperms in microscopic images especially in semen specimens with high density of sperms.

References

1. Fritz MA, Speroff L. Clinical Gynecologic Endocrinology and Infertility: Wolters Kluwer Health; 2012.
2. Jequier AM. Male Infertility: A Clinical Guide: Cambridge University Press; 2011.
3. Allamaneni SS, Bandaranayake I, Agarwal A. Use of semen quality scores to predict pregnancy rates in couples undergoing intrauterine insemination with donor sperm. Fertil Steril. 2004 Sep;82(3):606-11.
4. Eliasson R. Semen analysis with regard to sperm number, sperm morphology and functional aspects. Asian J Androl. 2010;12(1):26-32.
5. Oku H, Ishikawa M, Ogawa N, Shiba K, Yoshida M. How to track spermatozoa using high-speed visual feedback. Conf Proc IEEE Eng Med Biol Soc. 2008; 2008:125-8.
6. Wenzhong Y, Shuqun S. Automatic Chromosome Counting Algorithm Based on Mathematical Morphology. Journal of Data Acquisition & Processing. 2008; 23(9):1004-9037.
7. Abbiramy VS, Shanthi V, Allidurai C, editors. Spermatozoa detection, counting and tracking in video streams to detect asthenozoospermia. Signal and Image Processing (ICSIP), 2010 International Conference on; 2010 15-17 Dec. 2010.
8. Berezansky M, Greenspan H, Cohen-Or D, Nunez J, Eitan O. Segmentation and tracking of human sperm cells using spatiotemporal representation and clustering. Proceedings of the SPIE. 2007 March; 6512(2): 65122M.
9. Soler C, de Monserrat JJ, Gutierrez R, Nunez J, Nunez M, Sancho M, et al. Use of the Sperm-Class Analyser for objective assessment of human sperm morphology. Int J Androl. 2003 Oct;26(5):262-70.
10. Shi LZ, Nascimento JM, Chandsawangbhuwana C, Botvinick EL, Berns MW. An automatic system to study sperm motility and energetics. Biomed Microdevices. 2008 Aug; 10(4):573-83.
11. Leung C, Lu Z, Esfandiari N, Casper RF, Sun Y. Automated sperm immobilization for intracytoplasmic sperm injection. Biomedical Engineering, IEEE Transactions on. 2011; 58(4):935-42.
12. Zheng L, Wang Y,. The sperm video segmentation based on dynamic threshold. Machine Learning and Cybernetics, 2010 Proceedings of the 9th International Conference on; 2010: IEEE. [13] Carrillo H, Villarreal J, Sotaquira M, Goelkel M, Gutierrez R, editors. A computer aided tool for the assessment of human sperm morphology. Bioinformatics and Bioengineering, 2007 BIBE 2007 Proceedings of the 7th IEEE International Conference on; 2007: IEEE.
13. Alias MF, Isa NAM, Sulaiman SA, Zamli KZ, editors. Detection of Sprague Dawley Sperm Using Matching Method. Knowledge-Based Intelligent Information and Engineering Systems; 2008: Springer.
14. Shojaedini V, Kermani A, and Nafisi V, A New Method for Sperms Detection in Human Semen: Combination of Hypothesis Testing and Local Mapping of Wavelet Sub-Bands. Iran J Med Phys. 2012;9:283-92.
15. Abbiramy V, Shanthi V. Spermatozoa segmentation and morphological parameter analysis based detection of teratozoospermia. International Journal of Computer Applications. 2010;3(7):19-23.
16. Baraldi A, Parmiggiani F. An investigation of the textural characteristics associated with GLCM matrix statistical parameters. Geoscience and Remote Sensing. IEEE Transactions on. 1995;33(2):293-304.
17. Kekre H, Thepade SD, Sarode TK, Suryawanshi V. Image Retrieval using Texture Features extracted from GLCM, LBG and KPE. International Journal of Computer Theory and Engineering. 2010;2(5):1793-8201.

18. Horng M-H. Multilevel minimum cross entropy threshold selection based on the honey bee mating optimization. Expert Systems with Applications. 2010; 37(6):4580-92.
19. Pal NR, Pal SK. Image model, Poisson distribution and object extraction. International journal of pattern recognition and artificial intelligence. 1991;5(03):459-83.
20. Lee S, Lo C, Wang C, Chung P, Chang C, Yang C, et al. A computer-aided design mammography screening system for detection and classification of microcalcifications. Int J Med Inform. 2000 Oct;60(1):29-57.
21. Roerdink JB, Meijster A. The watershed transform: Definitions, algorithms and parallelization strategies. Fundamenta Informaticae. 2000;41(1):187-228.
22. Bieniek A, Moga A. An efficient watershed algorithm based on connected components. Pattern Recognition. 2000;33(6):907-16.
23. Bai W, Liu J, Chen G. Segmentation of white rat sperm image. Parallel Processing of Images and Optimization and Medical Imaging Processing, 2011 Proceedings of; 2011: SPIE.